nature medicine

Comprehensive volumetric optical microscopy *in vivo*

Seok H Yun[1,2], Guillermo J Tearney[1,3,4], Benjamin J Vakoc[1,2], Milen Shishkov[1,2], Wang Y Oh[1,2], Adrien E Desjardins[1,4,5], Melissa J Suter[1,2], Raymond C Chan[1,6], John A Evans[1,7], Ik-Kyung Jang[8], Norman S Nishioka[1,4,7], Johannes F de Boer[1,2,4] & Brett E Bouma[1,2,4]

Comprehensive volumetric microscopy of epithelial, mucosal and endothelial tissues in living human patients would have a profound impact in medicine by enabling diagnostic imaging at the cellular level over large surface areas. Considering the vast area of these tissues with respect to the desired sampling interval, achieving this goal requires rapid sampling. Although noninvasive diagnostic technologies are preferred, many applications could be served by minimally invasive instruments capable of accessing remote locations within the body. We have developed a fiber-optic imaging technique termed optical frequency-domain imaging (OFDI) that satisfies these requirements by rapidly acquiring high-resolution, cross-sectional images through flexible, narrow-diameter catheters. Using a prototype system, we show comprehensive microscopy of esophageal mucosa and of coronary arteries *in vivo*. Our pilot study results suggest that this technology may be a useful clinical tool for comprehensive diagnostic imaging for epithelial disease and for evaluating coronary pathology and iatrogenic effects.

Many important diseases arise from and exist within superficial tissue layers. For example, epithelial metaplasia, dysplasia and early cancers may be found in luminal organ mucosa, and high-risk coronary atherosclerotic plaques occupy the intima. Finding these lesions can be difficult, however, as they are characterized by microscopic features not visible to the eye and may be focally and heterogeneously distributed over a large luminal surface area. A catheter or endoscope capable of comprehensively conducting microscopy in patients over large surface areas and throughout the entire mucosa or intima could provide new possibilities for early diagnosis and characterization of these prevalent diseases.

Optical biopsy has recently been championed for nonexcisional histopathologic diagnosis *in situ*, but three-dimensional microscopy over large mucosal or intimal volumes remains a challenge. Confocal microscopy provides cellular resolution in tissue up to a depth of several hundred microns *in vivo*[1]. The limited field of view, similar to that of high-magnification microscopy, and the challenge of engineering small-diameter endoscopes[2], however, make comprehensive three-dimensional imaging difficult. Optical coherence tomography (OCT)[3], with resolution ranging from 2 μm to 15 μm, is also capable of imaging microscopic structure in individuals. Its inherent vertical cross-sectional imaging capabilities and relative ease of incorporation into fiber-optic catheters and endoscopes[4] make it a promising candidate for comprehensive volumetric microscopy. Human studies have shown that OCT is capable of identifying dysplasia in Barrett's esophagus[5] and colonic adenomas[6] and can identify all of the histopathologic features of vulnerable coronary plaques[7]. Until now, however, OCT has been too slow for comprehensive microscopic imaging, and it has therefore been relegated to a point-sampling technique with a field of view comparable to that in conventional biopsy. Recently, it has been shown that the application of frequency-domain ranging techniques[8,9], instead of the delay-scanning interferometry of OCT, substantially improves detection sensitivity[10–12]. This new approach, optical frequency-domain imaging (OFDI)[13], leverages high sensitivity to provide imaging speed that is orders of magnitude faster than that in conventional OCT. Here, we present the first catheter-based images obtained with OFDI *in vivo* and show the potential of this technology for rapidly imaging large tissue volumes at microscopic resolution.

RESULTS

We performed comprehensive volumetric microscopy with OFDI using minimally invasive catheterization and endoscopy to deliver the fiber-optic probe to the target organ or organ system (**Fig. 1**). The OFDI probe delivers infrared laser light and collects photons that are back-scattered from refractive-index inhomogeneities of microscopic structures within the tissue. We determined the intensity and origin of the reflected light by detecting spectrally resolved interference as the source laser wavelength was tuned[9,13]. Through rapid rotation and longitudinal pull-back of the internal portion of the probe, the OFDI system records the full three-dimensional microstructure of the tissue. We then used image processing to render volumetric images and to provide a form of virtual histology, in which high-resolution cross-sectional views of arbitrary locations in the tissue can be obtained. The prototype OFDI systems (**Supplementary Fig. 1** online) developed for these studies

[1]Wellman Center for Photomedicine, 55 Fruit Street; [2]Department of Dermatology; and [3]Department of Pathology, Harvard Medical School and Massachusetts General Hospital, Boston, Massachusetts 02114, USA. [4]Harvard-MIT Division of Health Sciences and Technology, 77 Massachusetts Avenue, Cambridge, Massachusetts 02139, USA. [5]Biophysics Program, Harvard University, Cambridge, Massachusetts 02138, USA. [6]Department of Radiology, [7]Department of Gastroenterology, and [8]Department of Cardiology, Harvard Medical School and Massachusetts General Hospital, Boston, Massachusetts 02114, USA. Correspondence should be addressed to B.E.B. (bouma@helix.mgh.harvard.edu).

Received 15 March; accepted 20 June; published online 19 November 2006; doi:10.1038/nm1450

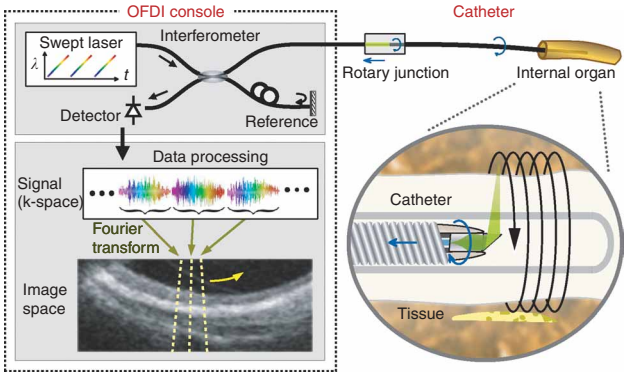

Figure 1 Principles of comprehensive optical frequency-domain imaging (OFDI). Minimally invasive catheters or endoscopes provide for access of the optical fiber to the organ or system of interest. An optical beam is focused into the tissue, and the echo-time delay and amplitude of light reflected from the tissue microstructure at different depths are determined by detecting spectrally resolved interference between the tissue sample and a reference, as the source laser wavelength is rapidly varied from 1,264 nm to 1,376 nm. A Fourier transform of this signal forms image data along the axial line (A-line), which is determined by the optical beam emitted from the probe. A-lines are continuously acquired as the probe is actuated to provide spatial scanning of the beam in two directions that are orthogonal to the axial line (rotational and pull-back motion by a rotary junction). The resulting three-dimensional data sets can be rendered and viewed in arbitrary orientations for gross screening, and individual high-resolution cross-sections can be displayed at specific locations of interest.

provided an approximately 30-fold increase in A-line acquisition rate (up to 64,000 axial image lines per s) and a 3-fold increase in ranging depth (7.3 mm in air) over conventional OCT systems, corresponding to a 90-fold increase in imaging speed. These technical advances, combined with the use of high-speed rotational catheters, enabled imaging *in vivo* over large tissue areas (>25 cm^2) and depths (up to 2 mm), with a three-dimensional resolution of approximately 15 μm × 15 μm × 10 μm.

Upper gastrointestinal tract imaging *in vivo*

To show the potential of OFDI for comprehensive volumetric microscopy, we imaged the esophagus of two female Yorkshire swine *in vivo* using a cylindrical balloon OFDI catheter. The entire volume of data in a 4.5-cm-long segment of each swine esophagus was acquired in 5.8 min (**Fig. 2** and **Supplementary Video 1** online). As the complete 14-GB data set cannot be encapsulated in discrete figures, here we present data after compression and downsampling. Volumetric renderings depict the tubular anatomy and allow visualization of the vascular network supplying the esophagus (**Fig. 2a**). We measured the longitudinal length of the volumetric image directly using a pull-back encoder and confirmed this measurement by visualization of the balloon's terminal ends, which were separated by 4.5 cm (data not shown). We obtained the radial dimension using interferometry and confirmed it by imaging the diameter of the balloon (1.8 cm). The volumetric data allowed us to render two-dimensional cross-sections in longitudinal (**Fig. 2b**) and circumferential (**Fig. 2c**) directions.

We acquired a total of ten volumetric images in two swine with no complications or instrument failures. As the physical characteristic of tissues that gives rise to image contrast, optical scattering, is identical in OCT and OFDI, we applied interpretation criteria that have been established for OCT (refs. 14,15) to identify anatomical structures in the OFDI images (**Fig. 2d**). The architectural assignments were supported by corresponding histological sections that we acquired after the imaging procedures (**Fig. 2e**). The dimension and optical properties of these anatomical features are similar in swine and humans[14].

Intracoronary imaging *in vivo*

Intravascular optical imaging is particularly challenging as blood cells cause scatter light and degrade coherence. One solution to this challenge is to temporarily displace blood by injecting saline at the coronary ostium. Previous studies with OCT have shown that this approach can provide several seconds of clear viewing without ischemia or other complications[16,17]. With sufficiently fast imaging, therefore, long segments of coronaries could be comprehensively imaged during saline injection. Using a prototype OFDI system operating at an A-line acquisition rate of 54 kHz (108 images per s), we acquired volumetric data sets in each

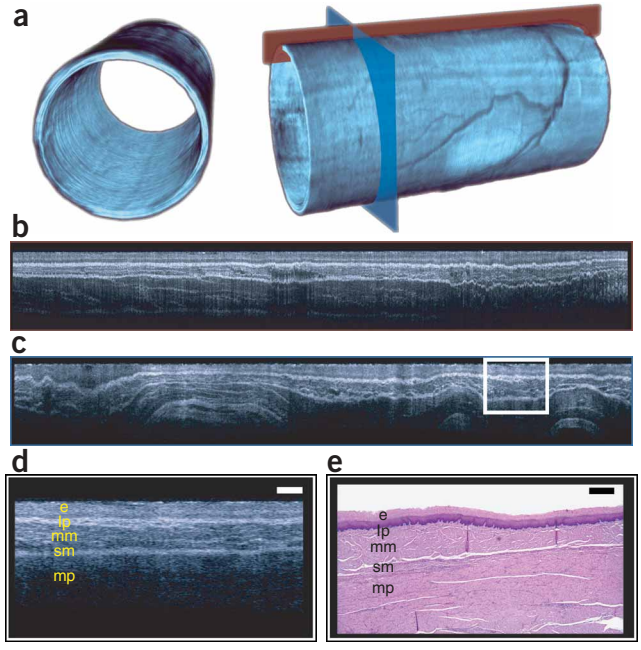

Figure 2 Comprehensive microscopy of a porcine esophagus *in vivo*. (**a**) The 14-GB volumetric data set was rendered and downsampled for presentation in arbitrary orientations and perspectives. The vascular network within the submucosa is readily apparent without image enhancement or exogenous contrast agents. Cross-sectional images can be located on the volume image for higher-resolution viewing. (**b**) Longitudinal cross-section through esophageal wall at location denoted in **a** (inverted with epithelium at the top; dimensions: 45 mm horizontal, 2.6 mm vertical). In the raw data, we observed a periodic vertical offset corresponding to the motion of the beating heart. We used a simple surface-aligning algorithm to reduce this artifact, but a residual vertical banding can still be observed with a period of 300 μm corresponding to a heart rate of 90 beats/min. The longitudinal spacing between adjacent A-lines was 32 μm. (**c**) Unwrapped transverse section (cylindrical coordinates r and θ are mapped to vertical and horizontal) at location denoted in **a** (dimensions: 57 mm horizontal, 2.6 mm vertical). Both sections show imaging through the entire esophageal wall. (**d**) Magnification of boxed area in **c**, showing the squamous epithelium (e), lamina propria (lp), muscularis mucosa (mm), submucosa (sm) and muscularis propria (mp). (**e**) Representative histology section (H&E stain) obtained from the anatomical region corresponding to that depicted in **d**. Scale bars, 500 μm.

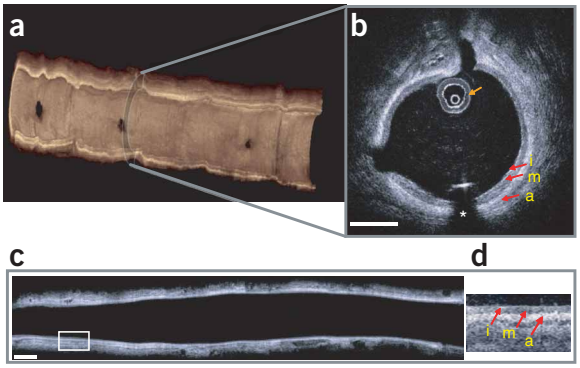

Figure 3 Comprehensive microscopy of a porcine coronary artery *in vivo*. (**a**) Three-dimensional cut-away rendering of the volumetric data set acquired with an intravascular catheter in the right coronary artery of a living swine. The volume comprises 400 circular (*r*-θ) sections at a spacing of 50 μm acquired in 3.7 s during the injection of saline at a rate of 3 ml/s. The ostia of three side branches can be clearly seen. (**b**) A single circular cross-section at the location denoted in **a**. The opaque guidewire and the sector that it obscures are denoted by the asterisk. Orange arrow indicates image of the transparent catheter sheath. Red arrows designate intima (i), media (m) and adventitia (a). (**c**) A longitudinal section rendered from the volumetric data, using a spatial low-pass filtering of the surface and subsequent surface alignment to reduce spatial distortion arising from pulsation. (**d**) Magnification of boxed area in **c**, showing trilaminar structure of vessel wall in longitudinal perspective. Image data was acquired at a rate of 108 frames/s. Scale bars, 1 mm.

of the three main coronary arteries in five living swine. We automated saline delivery using an infusion pump and injection rates of 2–4 ml/s. The internal core of the catheters rotated at a rate of 108 revolutions per s, and a computer-controlled translation stage provided longitudinal (pull-back) actuation. We obtained a total of 56 volumetric data sets: 22 in the right coronary artery, 10 in the left anterior descending artery and 24 in the circumflex artery. In four scans, flushing did not provide clear viewing of the artery wall. In an additional eight volumetric scans, we found that the catheter used contained a fractured optical fiber, which led to excessive optical attenuation. The remaining 44 scans yielded clear visualization of the entire arterial wall over coronary segment lengths ranging from 24.3 mm to 63.3 mm. A three-dimensional rendering of a right coronary artery showed side-branch ostia consistent with the gross appearance of a typical prosected artery (**Fig. 3a** and **Supplementary Video 2** online). The volumetric data could also be viewed in arbitrary circular (**Fig. 3b**) or longitudinal (**Fig. 3c**) sections for clear examination of the structure of the vessel wall, including the single-cell-layer intima, media and adventitia as indicated by the image interpretation criteria[7] established with OCT. Although the optical properties of these layers are similar in humans and swine[16], our previous studies with OCT found substantial pathologic thickening and a richer, more heterogeneous structure in human subjects[17] (**Supplementary Video 3** online).

Imaging following angioplasty and stenting

In addition to imaging normal coronary arteries, we conducted a feasibility study to assess the potential of OFDI for imaging disrupted arterial structure. We performed angioplasty and stenting in the circumflex artery of one swine. During the angioplasty procedure, we over-inflated a balloon catheter intentionally in order to induce partial dissection of the arterial wall. We then positioned a coronary stent to partially overlap the dissected region. A volumetric OFDI image, acquired after stenting (**Fig. 4**), delineates the metallic wire mesh of the stent, the intima and media, and the remainder of the vessel and surrounding tissues including denuded adventitia. The luminal diameter is considerably expanded relative to the reference vessel diameters. The wire struts of the stent are opaque to infrared light and appear as bright local reflections at the lumen with occluded sectors radially behind them[18]. Cross-sectional images revealed portions of the dissected intima and media inside the stent (**Fig. 4c**,**d**), and the exposed adventia and flaps of the intima and media (**Fig. 4d**,**e**). After an interval of approximately 15 min, we acquired an additional volumetric data set and observed thrombi at locations of disrupted intima and media (**Fig. 5** and **Supplementary Video 4** online).

DISCUSSION

Comprehensive volumetric microscopy could bridge the gap between noninvasive radiologic techniques, which provide wide-field imaging but lack sufficient resolution for cellular diagnosis, and point-sampling approaches such as excisional biopsy. Previous research has shown the diagnostic potential of OCT, but, because of the relatively slow imaging speed, wide-field screening has not been feasible. We have shown that by acquiring the interferometric signal of OCT in the frequency domain using a wavelength-swept laser source, detection sensitivity can be markedly improved and the imaging of large luminal areas can be readily performed using minimally invasive, narrow-diameter catheter probes.

The diagnosis of epithelial cancers and their precursors exemplifies the need for comprehensive volumetric microscopy. As these lesions

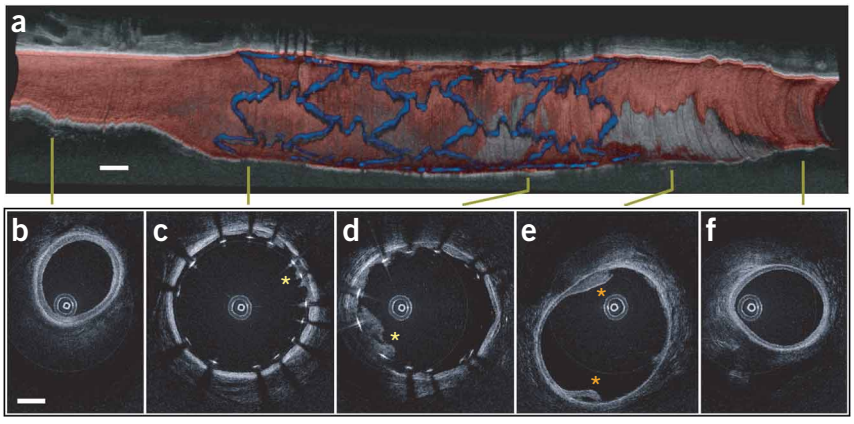

Figure 4 Volumetric imaging of a stented porcine coronary artery *in vivo*. (**a**) Three-dimensional cut-away rendering of the volumetric data set acquired with an intravascular catheter in the circumflex coronary artery of a living swine after balloon angioplasty and stent implantation. Blue, stent; red, intima and media; gray, adventia and surrounding tissue. The volume comprises 500 circular (*r*-θ) sections at a spacing of 50 μm acquired in 6 s during the injection of saline at 3 ml/s. (**b**–**f**) Individual OFDI cross-sectional images at the five locations marked in **a**. The metal-based stent produces strongly reflected signals and leaves radial shadow patterns in **c** and **d**. The dissected intima and media layers are shown (**e**; orange asterisk). Tissue prolapse between the stent struts is visualized in **c** and **d** (yellow asterisk). Scale bars, 1 mm.

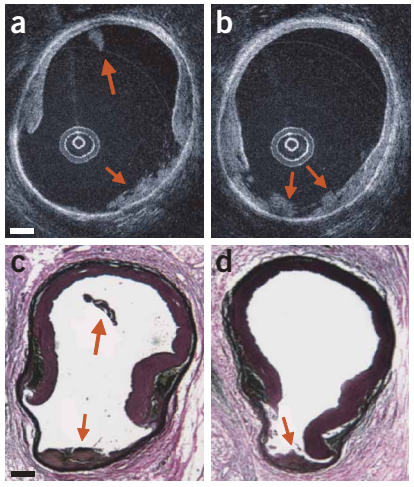

Figure 5 Cross-sectional images of dissected coronary artery and histology comparison. (**a**,**b**) Circular cross-sectional OFDI images acquired 15 min after stent deployment at the stent border (**a**), and 1.0 mm distal to the stent (**b**). Disruption of the intima and media is evident, as well as thrombus (arrows). (**c**,**d**) Histology sections (elastin stain) obtained at locations corresponding to those depicted in **a** and **b**, respectively, showing similar features of disruption and thrombus. Scale bars, 500 μm.

are frequently focal and can be distributed heterogeneously across a wide field, sensitive diagnosis is extremely demanding; diagnosis must be rendered on a microscopic scale over areas larger than 10 cm^2. Barrett's esophagus is a clinically important condition because it is a precursor of esophageal adenocarcinoma, a cancer associated with high morbidity and a dismal prognosis. Previous preliminary clinical studies have shown that conventional OCT imaging can identify high-grade dysplasia and adenocarcinoma when used in a point-sampling mode similar to random biopsy[19]. As image resolution and contrast in OCT and OFDI are identical, OCT diagnostic criteria[5,19] for focal diagnosis of Barrett's esophagus, dysplasia and intramucosal adenocarcinoma should be directly applicable to OFDI. With the current OFDI prototype, the time required for comprehensively imaging the distal esophagus was less than 6 min. Although this duration may be acceptable for clinical use, shorter procedure times would be attractive. The use of a higher speed computer bus and parallel hard drives may support the use of the OFDI system at an A-line acquisition rate of 68 kHz, which would reduce procedure times to less than 1 min.

A second category of applications for comprehensive volumetric microscopy is the diagnosis and characterization of superficial disease in cases where excisional biopsy is hazardous. The hypothesis of a vulnerable plaque is one of the most important current topics in interventional cardiology[20]. Autopsy studies have found that most acute myocardial infarctions are secondary to thrombotic occlusion at the site of a disrupted lipid-rich plaque, characterized by large necrotic, lipid-rich cores, thin fibrous caps and abundant macrophages[21]. It is hypothesized that this type of coronary plaque places patients at a greater risk for heart attack[22]. To test this hypothesis, develop appropriate therapeutic measures and potentially guide intervention, there is a clear need for diagnostic methods capable of identifying these lesions in living individuals before plaque rupture. The combination of previously validated OCT criteria for the focal characterization of coronary atherosclerotic plaques[7,23,24] with comprehensive intracoronary OFDI may meet this need.

The coherent detection used in OCT and OFDI cannot directly detect fluorescence. Several molecular contrast methods, however, have already been suggested for conventional OCT, such as coherent antistokes Raman shift[25] and protein-based probes[26]. Extension of these techniques to OFDI will enhance its utility in biomedical research, as well as in clinical medicine. Furthermore, functional techniques, including Doppler[27] and polarization-sensitive[28] methods, provide further contrast mechanisms that may be used for the study of disease and for primary diagnosis.

METHODS

OFDI data acquisition and processing. OCT and OFDI use interferometry to measure the same physical entity, the electric field amplitude, $A_S(z)$, of light reflected from a depth z within the sample S. Images are then produced by mapping $A_S(x,y,z)$, obtained through multiple axial scans, to a grayscale lookup table. The interferometric signal in OFDI, $S(k,z_0)$, at optical wavenumber k ($= 2\pi/\lambda$, where λ = wavelength) and reference delay length z_0, can be expressed as $S(k,z_0) = \int A_R A_S(z) cos[k(z-z_0)]dz$, where A_R denotes the amplitude of reference light. This signal is collected while holding z_0 constant and while varying k using a monochromatic laser whose wavelength varies over time. $A_S(z)$ is computed through Fourier transformation: $A_S(z) = \frac{1}{A_R}\int S(k,z_0) cos[k(z-z_0)]dk$. Thus, A_S is detected at all depth points simultaneously. In OCT, a broadband light source is used and the detector integrates over k-space; the directly measured signal is $\int S(k,z_0)dk = A_R A_S(z_0)$. The full depth dependence of A_S is then captured sequentially by scanning z_0. Although the displayed image is a graphical presentation of $A_S(z)$ in both OCT and OFDI, the Fourier integration in OFDI processing enhances the detection sensitivity several hundred times. Additionally, as depth scanning is not required in OFDI, this improvement in sensitivity can be leveraged to increase imaging speed.

OFDI systems. At the core of the OFDI systems (**Supplementary Fig. 1**) is a unique laser source that uses a semiconductor optical amplifier (Covega) and custom-made filter based on a polygonal scanner (Lincoln Laser)[29]. The laser developed for this study provided a sweep range of 111 nm (1,264–1,376 nm), repetition rate of 64 kHz and average power of 30 mW. The fiber-optic core of the systems is also unique in that it provides dual-balanced and polarization-diverse detection along with an acousto-optic frequency shifter (Brimrose) that removes depth degeneracy and doubles the effective ranging depth. The large ranging depth of 7.3 mm of our system accommodates varying distances between the OFDI probe and the tissue surface. The electrical signals from the detectors are digitized with a two-channel analog-to-digital converter (Gage Applied Technologies) at a sampling rate of 100 MHz.

Gastrointestinal imaging. We developed a custom catheter comprising a rotating optical core and balloon sheath for centration within the esophageal lumen. We performed esophageal imaging in two anaesthetized female Yorkshire swine weighing approximately 35 kg, according to a protocol approved by the Massachusetts General Hospital Subcommittee on Research Animal Care. No effort was made to flush mucus from the esophageal wall before balloon inflation. We operated the imaging system at a reduced A-line acquisition rate of 10 kHz, to facilitate streaming the acquired data continuously to a storage medium (using a standard data bus in a personal computer). The system acquired a total of 3,500,000 axial profiles over 5.8 min while rotating and translating the catheter to provide a longitudinal spacing of 32 μm between adjacent circular cross-sections.

Coronary imaging. We fabricated OFDI imaging catheters (0.8 mm diameter) based on a design similar to that of commercial intracoronary ultrasound imaging catheters. We performed coronary imaging in five female Yorkshire swine (40–50 kg) according to a protocol approved by the Massachusetts General Hospital Subcommittee on Research Animal Care. After anesthesia and heparin administration (100 U per kg body weight intravenously), we inserted a 7F guide catheter into the right femoral artery and advanced it over a guide wire to the distal coronary artery while monitoring the catheter's position by angiography. To displace blood from the field of view, we delivered saline through the guide catheter using an injection pump (MedRad) at a constant rate of 2–4 ml/s. The imaging system continuously acquired data at an A-line rate of 54 kHz and temporarily streamed these data to a 2-GB digital memory

on the acquisition board itself. The rotary junction rotated the inner core of the catheter at 108 revolutions/s and pulled the core longitudinally within the sheath with a velocity 5.4–16.2 mm/s. Each volumetric image comprised a total of 680 cross-sectional frames (500 radial A-lines per frame) and was acquired over 6.3 s. The longitudinal spacing of the volumetric imaging ranged from 50 μm to 150 μm.

Angioplasty and stent deployment. Before the balloon was inflated, the lumen diameter was 3.3 mm. We inflated the balloon to a diameter of 4.0 mm in order to intentionally induce partial dissection of the arterial wall. We then positioned a 13-mm-long coronary stent and expanded it to a diameter of 3.9 mm using 20 atm of pressure. We acquired OFDI images immediately after stent deployment and following an interval of approximately 15 min, starting from the distal circumflex and extending to the normal segment of artery proximal to the stent. After the entire procedure, we prosected the circumflex artery and obtained histology sections 5 mm proximal to the stent and at three distal locations with intervals of 1.0 mm starting at the distal border of the stent.

Note: Supplementary information is available on the Nature Medicine website.

ACKNOWLEDGMENTS

This research was supported in part by the US National Institutes of Health (contracts R01 HL070039, R33 CA110130, R01 RR0119768, R01 HL076398 and R01 CA103769) and by the Terumo Corporation.

COMPETING INTERESTS STATEMENT

The authors declare that they have competing financial interests (see the *Nature Medicine* website for details).

Published online at http://www.nature.com/naturemedicine/
Reprints and permissions information is available online at http://npg.nature.com/reprintsandpermissions/

1. Rajadhyaksha, M., Gonzalez, S., Zavislan, J.M., Anderson, R.R. & Webb, R.H. *In vivo* confocal scanning laser microscopy of human skin II: advances in instrumentation and comparison with histology. *J. Invest. Dermatol.* **113**, 293–303 (1999).
2. Kiesslich, R. *et al.* Confocal laser endoscopy for diagnosing intraepithelial neoplasias and colorectal cancer *in vivo*. *Gastroenterology* **127**, 706–713 (2004).
3. Huang, D. *et al.* Optical coherence tomography. *Science* **254**, 1178–1181 (1991).
4. Tearney, G.J. *et al.* Optical biopsy in human gastrointestinal tissue using optical coherence tomography. *Am. J. Gastroenterol.* **92**, 1800–1804 (1997).
5. Poneros, J.M. *et al.* Diagnosis of specialized intestinal metaplasia by optical coherence tomography. *Gastroenterology* **120**, 7–12 (2001).
6. Pfau, P.M. *et al.* Criteria for the diagnosis of dysplasia by endoscopic optical coherence tomography. *Gastrointest. Endosc.* **58**, 196–202 (2003).
7. Yabushita, H. *et al.* Characterization of human atherosclerosis by optical coherence tomography. *Circulation* **106**, 1640–1645 (2002).
8. Kingsley, S.A. & Davies, D.E.N. OFDR diagnostics or fibre and integrated-optic systems. *Electron. Lett.* **21**, 434–435 (1985).
9. Fercher, A.F., Hitzenberger, C.K., Kamp, G. & El-Zaiat, S.Y. Measurement of intraocular distances by backscattering spectral interferometry. *Opt. Commun.* **117**, 43–45 (1995).
10. Leitgeb, R., Hitzenberger, C.K. & Fercher, A.F. Performance of Fourier domain vs. time domain optical coherence tomography. *Opt. Express* **11**, 889–894 (2003).
11. de Boer, J.F. *et al.* Improved signal-to-noise ratio in spectral-domain compared with time-domain optical coherence tomography. *Opt. Lett.* **28**, 2067–2069 (2003).
12. Choma, M.A., Sarunic, M.V., Changhuei, Y. & Izatt, J.A. Sensitivity advantage of swept source and Fourier domain optical coherence tomography. *Opt. Express* **11**, 2183–2189 (2003).
13. Yun, S.H., Tearney, G.J., de Boer, J.F., Iftimia, N. & Bouma, B.E. High-speed optical frequency-domain imaging. *Opt. Express* **11**, 2953–2963 (2003).
14. Bouma, B.E., Tearney, G.J., Compton, C.C. & Nishioka, N.S. High-resolution imaging of the human esophagus and stomach *in vivo* using optical coherence tomography. *Gastrointest. Endosc.* **51**, 467–474 (2000).
15. Kobayashi, K., Izatt, J.A., Kulkarni, M.D., Willis, J. & Sivak, M.V. High-resolution cross-sectional imaging of the gastrointestinal tract using optical coherence tomography: preliminary results. *Gastrointest. Endosc.* **47**, 515–523 (1998).
16. Jang, I.K. *et al.* Visualization of coronary atherosclerotic plaques in patients using optical coherence tomography: comparison with intravascular ultrasound. *J. Am. Coll. Cardiol.* **39**, 604–609 (2002).
17. Jang, I.K. *et al. In vivo* characterization of coronary atherosclerotic plaque using optical coherence tomography. *Circulation* **111**, 1551–1555 (2005).
18. Bouma, B.E. *et al.* Evaluation of intracoronary stenting by intravascular optical coherence tomography. *Heart* **89**, 317–321 (2003).
19. Evans, J.A. *et al.* Optical coherence tomography to identify intramucosal carcinoma and high-grade dysplasia in Barrett's esophagus. *Clin. Gastroenterol. Hepatol.* **4**, 38–43 (2006).
20. Libby, P. Inflammation in atherosclerosis. *Nature* **420**, 868–874 (2002).
21. Davies, M.J. Stability and instability: two faces of coronary atherosclerosis. The Paul Dudley White Lecture. *Circulation* **94**, 2013–2020 (1996).
22. Virmani, R., Kolodgie, F.D., Burke, A.P., Farb, A. & Schwartz, S.M. Lessons from sudden coronary death: a comprehensive morphological classification scheme for atherosclerotic lesions. *Arterioscler. Thromb. Vasc. Biol.* **20**, 1262–1275 (2000).
23. MacNeill, B.D. *et al.* Focal and multi-focal plaque macrophage distributions in patients with acute and stable presentations of coronary artery disease. *J. Am. Coll. Cardiol.* **44**, 972–979 (2004).
24. Tearney, G.J. *et al.* Quantification of macrophage content in atherosclerotic plaques by optical coherence tomography. *Circulation* **107**, 113–119 (2003).
25. Boppart, S.A., Oldenburg, A.L., Xu, C.Y. & Marks, D.L. Optical probes and techniques for molecular contrast enhancement in coherence imaging. *J. Biomed. Opt.* **10**, 41208 (2005).
26. Yang, C., Choma, M.A., Lamb, L.E. & Simon, J.D. Protein-based molecular contrast optical coherence tomography with phytochrome as the contrast agent. *Opt. Lett.* **29**, 1396–1398 (2004).
27. Vakoc, B.J., Yun, S.H., de Boer, J.F., Tearney, G.J. & Bouma, B.E. Phase-resolved optical frequency domain imaging. *Opt. Express* **13**, 5483–5493 (2005).
28. Zhang, J., Jung, W., Nelson, J.S. & Chen, Z. Full range polarization-sensitive Fourier domain optical coherence tomography. *Opt. Express* **12**, 6033–6039 (2004).
29. Yun, S.H., Boudoux, C., Tearney, G.J. & Bouma, B.E. High-speed wavelength-swept semiconductor laser with polygon-scanner-based wavelength filter. *Opt. Lett.* **28**, 1981–1983 (2003).